G-band resonant Raman study of 62 isolated single-wall carbon nanotubes

A. Jorio,[1,2] A. G. Souza Filho,[1,3] G. Dresselhaus,[4] M. S. Dresselhaus,[1,5] A. K. Swan,[6] M. S. Ünlü,[6] B. B. Goldberg,[6,7] M. A. Pimenta,[2] J. H. Hafner,[8,*] C. M. Lieber,[8] and R. Saito[9]

[1]*Department of Physics, Massachusetts Institute of Technology, Cambridge, Massachusetts 02139-4307*

[2]*Departamento de Física, Universidade Federal de Minas Gerais, Belo Horizonte, MG, 30123-970 Brazil*

[3]*Departamento de Física, Universidade Federal do Ceará, Fortaleza - CE, 60455-760 Brazil*

[4]*Francis Bitter Magnet Laboratory, Massachusetts Institute of Technology, Cambridge, Massachusetts 02139-4307*

[5]*Department of Electrical Engineering and Computer Science, Massachusetts Institute of Technology, Cambridge, Massachusetts 02139-4307*

[6]*Electrical and Computer Engineering Department, Boston University, Boston, Massachusetts 02215*

[7]*Department of Physics, Boston University, Boston, Massachusetts 02215*

[8]*Department of Chemistry, Harvard University, Cambridge, Massachusetts 02138*

[9]*Department of Electronic Engineering, University of Electro-Communications, Tokyo, 182-8585 Japan*

(Received 14 July 2001; revised manuscript received 12 October 2001; published 29 March 2002)

We report *G*-band resonance Raman spectra of single-wall carbon nanotubes (SWNTs) at the single-nanotube level. By measuring 62 different isolated SWNTs resonant with the incident laser, and having diameters d_t ranging between 0.95 nm and 2.62 nm, we have conclusively determined the dependence of the two most intense *G*-band features on the nanotube structure. The higher-frequency peak is not diameter dependent ($\omega_G^+ = 1591$ cm^{-1}), while the lower-frequency peak is given by $\omega_G^- = \omega_G^+ - C/d_t^2$, with C being different for metallic and semiconducting SWNTs ($C_M > C_S$). The peak frequencies do not depend on nanotube chiral angle. The intensity ratio between the two most intense features is in the range $0.1 < I_{\omega_G^-}/I_{\omega_G^+} < 0.3$ for most of the isolated SWNTs ($\sim$90%). Unusually high or low $I_{\omega_G^-}/I_{\omega_G^+}$ ratios are observed for a few spectra coming from SWNTs under special resonance conditions, i.e., SWNTs for which the incident photons are in resonance with the E_{44}^S interband transition and scattered photons are in resonance with E_{33}^S. Since the E_{ii} values depend sensitively on both nanotube diameter and chirality, the (n,m) SWNTs that should exhibit such a special *G*-band spectra can be predicted by resonance Raman theory. The agreement between theoretical predictions and experimental observations about these special *G*-band phenomena gives additional support for the (n,m) assignment from resonance Raman spectroscopy.

DOI: 10.1103/PhysRevB.65.155412 PACS number(s): 78.30.Na, 78.20.Bh, 63.22.+m

I. INTRODUCTION

The resonant Raman-scattering technique has been shown to provide a powerful tool for studying and characterizing single-wall carbon nanotubes (SWNTs),[1] for which the radial breathing mode (RBM) and the tangential mode vibrations (forming the so-called *G* band) are the two main features in the Raman spectra, with the resonant Raman spectra of the RBMs providing an easy and quick determination of the tube diameter distribution present in SWNT bundles.[2,3] The *G* band is a more complex spectral feature. Due to the folding of the graphite Brillouin zone into the SWNT zone, and due to the symmetry-breaking effects associated with the nanotube curvature, the E_{2g} peak in the Raman spectra of graphite splits into several modes with different symmetries in the Raman spectra of SWNTs.[4,5] Six modes [two $A(A_{1g})$, two $E_1(E_{1g})$, and two $E_2(E_{2g})$] are both predicted and observed to be Raman active in the *G* band of SWNTs.[6–14]

Experimental results show that the *G*-band profile for *semiconducting* SWNTs in the SWNT bundle is composed of basically four (sometimes five are observed) Lorentzian components.[1] The Raman spectra for *metallic* nanotubes in SWNT bundles exhibit only two strong peaks.[15–18] The higher-frequency mode ω_G^+ has a Lorentzian line shape, while the lower-frequency mode ω_G^- exhibits an asymmetric Breit-Wigner-Fano (BWF) line shape,[15,16,18] indicating coupling with an electronic continuum spectra.[18] This difference in line shape makes it possible to study separately the metallic and semiconducting SWNTs contained in a SWNT bundle, using different laser excitation energies E_{laser}.[1,19–21]

The general polarization behavior of aligned SWNTs is determined by the ''depolarization''[22] (or ''antenna'') effect, whereby light scattering is suppressed for light polarized perpendicular to the tube axes.[23–26] Symmetry assignments of the different phonon modes in *semiconducting* SWNTs were determined by polarized Raman experiments performed on a bundle of aligned SWNTs ($d_t = 1.85 \pm 0.25$ nm) using an excitation laser energy $E_{\text{laser}} = 2.41$ eV.[9] The *G*-band profile for semiconducting SWNTs in the SWNT bundle was deconvolved into four intrinsic SWNT components with the following symmetry assignments: $\omega_{E_2}^- \sim 1549$ cm^{-1} $[E_2(E_{2g})]$, $\omega_G^- \sim 1567$ cm^{-1} $[A(A_{1g}) + E_1(E_{1g})]$, $\omega_G^+ \sim 1590$ cm^{-1} $[A(A_{1g}) + E_1(E_{1g})]$, and $\omega_{E_2}^+ \sim 1607$ cm^{-1} $[E_2(E_{2g})]$.[9] For metallic SWNTs, the two features exhibit mostly *A* symmetry.[18]

Although there have been a considerable number of studies on the *G*-band feature regarding the difference in behavior between metallic and semiconducting nanotubes,[19–21] and regarding the dependence of the *G*-band spectra on polarization scattering geometries,[9,23–27] to our best knowledge, very

little is known about the dependence of the *G*-band spectra on nanotube structure, i.e., diameter d_t and chiral angle θ. Studies of the diameter dependence of the *G*-band mode frequencies were previously performed for both semiconducting[10] and metallic[18] SWNTs contained in bundles. However, since the SWNT bundles exhibit a distribution of tube diameters (more than 10%), and very few different bundles were measured (only three samples of SWNT bundles with different diameter distributions),[10,18] the results were not definitive. Chirality information is obviously not provided by bundle measurements.

The present paper is devoted to a study of the *G* band in the resonance Raman spectra of *isolated* SWNTs. We measured 62 different metallic and semiconducting SWNTs. The nanotube diameters can be obtained by the RBM frequency ($d_t = 248/\omega_{\mathrm{RBM}}$),[28] and a detailed study of the diameter dependence of the *G* band can be performed at the single-nanotube level.[29] Considering the two most intense features in the *G*-band spectra, we show that the highest-frequency peak ω_G^+ does not depend on the nanotube diameter, while the other intense feature ω_G^- appears at a lower frequency and its frequency increases with increasing tube diameter, showing a $1/d_t^2$ dependence, and extrapolating to ω_G^+ as $d_t \rightarrow \infty$. The splitting between the ω_G^+ and ω_G^- features is different for metallic and semiconducting SWNTs of the same diameter.

Making use of the tentative (n,m) assignment obtained by analysis of the RBM feature,[28] a detailed study of the chirality dependence of the *G* band can also be performed at the single-nanotube level. The tentative (n,m) assignment of the 62 SWNTs shows that neither ω_G^+ nor ω_G^- depends on nanotube chirality. Furthermore, regarding the intensity of the ω_G^+ and ω_G^- features, unusually high or low $I_{\omega_G^-}/I_{\omega_G^+}$ ratios are observed for a few spectra under special resonance conditions. This observation is closely related to the electronic transition values E_{ii} of these particular resonant SWNTs, and these special E_{ii} values are sensitively dependent on diameter and chiral angle. The (n,m) SWNTs that should exhibit such a special *G*-band spectra can be predicted by resonance Raman theory, and the agreement between theoretical predictions and experimental observations about this particular *G*-band effect gives additional support for the (n,m) assignment from resonant Raman spectroscopy.

II. EXPERIMENT

In this work we only discuss isolated SWNTs resonant with the *incident* light. In this case, the RBM, the *G* band and the *D* and G' bands are all present in the spectra and we can use the tentative (n,m) assignment from the RBM, *D*-band, and G'-band Raman features to analyze the *G*-band spectra systematically.[28,30,31] The use of a very dilute sample (~ 0.4 SWNT/μm^2) is important to be sure that when we observe, for example, the RBM feature and the *G* band in the same laser spot, both of these features come from the same SWNT. The probability of finding more than one resonant tube in the same light spot is very small, and much time must be spent on scanning the laser spot over the sample before finding a Raman signal from *any* SWNT that is in resonance with the laser excitation energy E_{laser}. The Raman spectra from 62 different isolated SWNTs, resonant with the incident laser light, were obtained in the present study. We tentatively assign the 62 SWNTs as 46 semiconducting and 16 metallic SWNTs. Three laser lines were used to obtain the Raman spectra from both metallic and semiconducting SWNTs over the diameter range present in the sample ($0.9 < d_t < 3.0$ nm). It is important to mention that we also have Raman spectra from more than 50 additional isolated SWNTs. These additional spectra were either obtained with a high-density sample (more than 1 SWNT/μm^2) or do not exhibit the RBM feature (which means that the resonance for the *G* band is with the scattered photon). These additional spectra are not directly considered in the present paper, but they are used to check the consistency of the present results.

Isolated SWNTs were prepared by a chemical vapor deposition (CVD) method on a slightly oxidized Si/SiO_2 substrate containing nanometer-size iron catalyst particles.[32] This procedure is more reliable than previously reported methods of sample preparation for single-nanotube spectroscopy,[23,25] since only isolated tubes are grown and no SWNT bundles are formed.[32] The nanotubes present on the Si/SiO_2 substrate were characterized by atomic force microscopy (AFM) and have diameters (d_t) ranging from 1 to 3 nm, and lengths ranging from a few hundred nanometers up to >2 μm. AFM images show that the sample has a very low nanotube density, containing only ~ 40 isolated nanotubes in a 100 μm^2 area.

The Raman spectra from isolated SWNTs on the Si/SiO_2 substrate were obtained using two Raman systems: a single monochromator Renishaw 1000B spectrometer equipped with a cooled charge coupled device detector and notch filters, and a Kaiser optical system, Hololab 5000R: a modular research micro-Raman spectrograph. The Raman spectra were collected in a backscattering configuration by a microscope using a 100$\times$ objective (laser spot ~ 1 μm). The 514.5 nm (2.41 eV) and the 488.0 nm (2.54 eV) lines from an Ar-ion laser, and the 785 nm (1.58 eV) line from a Ti:sapphire laser were used to obtain the Raman spectra. The laser power impinging on the substrate was ~ 10 mW.

III. *G*-BAND FREQUENCY DEPENDENCE ON SWNT DIAMETER

A. Experimental results

Figure 1 shows the RBM and the *G*-band Raman spectra for three isolated *semiconducting* SWNTs with different diameters d_t, at three different light spots on the substrate. The observed *G*-band spectra in Fig. 1 are typical of semiconducting SWNTs in bundles,[1] except that the spectra for isolated nanotubes exhibit much smaller linewidths (9 cm^{-1} compared to 20 cm^{-1} in SWNT bundles),[1] as shown in Fig. 1. The spectra here are displayed, from the top to the bottom, according to increasing RBM frequency (ω_{RBM}) [or decreasing SWNT diameter (d_t)]. Tentative (n,m) assignments[28,30,31] are used to label the data sets. The linewidth for the RBMs has been found in this work to be diam-

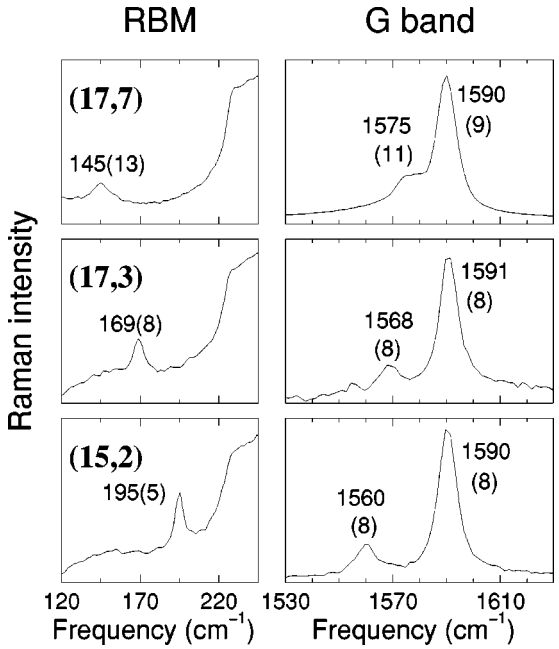

FIG. 1. The RBM and *G*-band Raman spectra for three isolated semiconducting SWNTs resonant with E_{laser}, that is, $E_{\text{laser}}=2.41$ eV for the spectrum in the top, labeled (17,7), and $E_{\text{laser}}=2.54$ eV for the other two spectra, labeled (17,3) and (15,2). The spectra are taken at three different spots on the substrate. The frequencies (linewidths) of the principal peaks for the RBM, ω_G^-, and ω_G^+ features are displayed in cm^{-1}. The shoulder observed to the right side of the RBM spectral feature comes from the Si substrate.

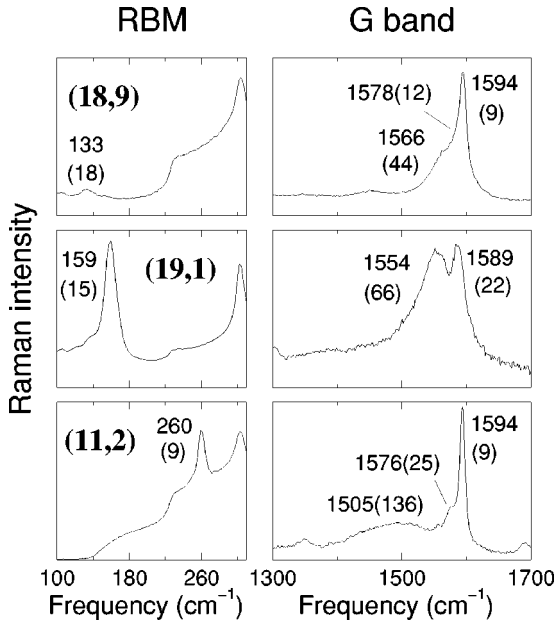

FIG. 2. The RBM and *G*-band Raman spectra for three isolated metallic SWNTs resonant with E_{laser}, that is, $E_{\text{laser}}=1.58$ eV for the spectrum labeled (19,1), and $E_{\text{laser}}=2.41$ eV for the other two spectra labeled (18,9) and (11,2). The spectra are taken at three different spots on the substrate. The frequencies (linewidths) of the peaks are displayed in cm^{-1}. The shoulder at 225 cm^{-1} and the peak at 303 cm^{-1} both come from the Si substrate.

eter dependent, decreasing with decreasing d_t. The *G*-band linewidth, however, does not exhibit any diameter dependence for this d_t range.

The *G*-band spectra in Fig. 2 for isolated *metallic* SWNTs are similar to the spectra observed for metallic SWNTs in bundles,[1] but the spectra at the single-nanotube level also show some differences in behavior. Figure 2 shows the RBM and the *G*-band Raman spectra for three isolated *metallic* SWNTs resonant with the laser at three different light spots on the sample. The spectra in Fig. 2 are displayed, from the top to the bottom, according to increasing ω_{RBM} [or decreasing SWNT diameter (d_t)]. The spectra in Fig. 2 are labeled by their tentatively assigned (n,m) indices.[28,30,31] The observation of a BWF peak for isolated SWNTs indicates that this line is an intrinsic feature of individual SWNTs. The BWF frequency decreases and the full width at half maximum intensity increases with decreasing d_t. Furthermore, a lower BWF intensity is observed for tubes with large d_t (upper spectrum in Fig. 2), i.e., smaller curvature. These results confirm the general dependence of the BWF line shape, previously reported for SWNT bundles containing SWNTs of different diameter ranges.[18] The $\omega_{\text{RBM}}=260$ cm^{-1} in the lowest spectrum in Fig. 2 [labeled (11,2)] comes from a relatively small diameter tube ($d_t=248/\omega_{\text{RBM}}=0.95$ nm), and this spectrum is quite similar to previously reported spectra for small diameter metallic tubes in SWNT bundles.[15]

In Fig. 3 we plot with filled circles the frequency vs $1/d_t$ for the two most intense *G*-band features (ω_G^- and ω_G^+) from the 46 isolated semiconducting SWNTs studied in the present work. The upper frequency ω_G^+ does not show a diameter-dependent behavior, but always appears at about 1591 cm^{-1} for the SWNT diameter range of the SWNTs in our sample. This is in agreement with several different resonance Raman measurements on SWNT bundles.[1] The lower-frequency ω_G^- mode, however, is diameter dependent and seems to extrapolate to 1591 cm^{-1} for $1/d_t \rightarrow 0$. The frequency of this mode can be very well fit with a simple equation $\omega_G^- = \omega_G^+ - C_S/d_t^2$, with the constants $C_S=47.7$ cm^{-1} nm^2 and $\omega_G^+ = 1591$ cm^{-1}. The deviation of the experimental points for ω_G^- from this curve (and from 1591 cm^{-1} in the case of ω_G^+) is less than ± 4 cm^{-1}. These results confirm that we observe the RBM and the *G* band from the same SWNTs in this very dilute isolated SWNT sample. The (less than ± 4 cm^{-1}) deviations of the experimental points from the $\omega_G^+ = 1591$ cm^{-1} or $\omega_G^- = 1591 - 47.7/d_t^2$ plots are probably due to nonintrinsic nanotube characteristics, such as bending of the tubes, roughness of the substrate surface, or the presence of defects or impurities. For SWNTs with diameters close to one another, we plotted (not shown) the *G*-band mode frequencies vs chiral angle (as tentatively determined by analyzing the RBM, *D*-band, and G'-band spectra),[28,30,31] and no dependence of ω_G^+ and ω_G^- on chirality was observed, in agreement with calculations using the tight-binding molecular-dynamics method.[11,12]

In Fig. 3 we plot with open circles the frequency vs $1/d_t$ for the higher-frequency Lorentzian peak ω_G^+ and for the

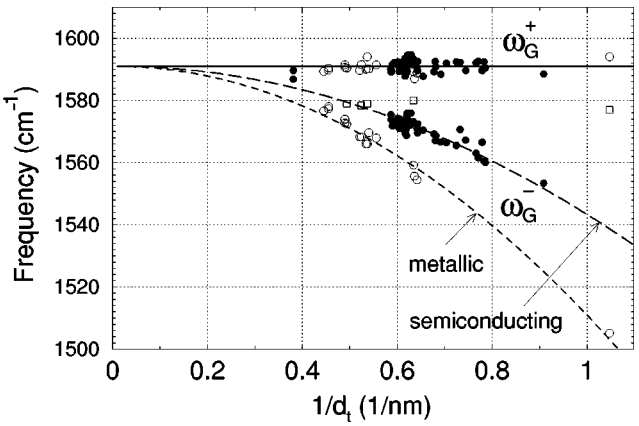

FIG. 3. ω_G^- and ω_G^+ for semiconducting (filled circles) and metallic (open circles) SWNTs are plotted as a function of $1/d_t$. The flat solid line shows $\omega_G^+ = 1591$ cm^{-1} independent of d_t, θ, and E_{laser}. The curves are given by the function $\omega_G^- = 1591 - C/d_t^2$, where $C = C_S = 47.7$ cm^{-1} nm^2 is for semiconducting SWNTs (long-dashed curve) and $C = C_M = 79.5$ cm^{-1} nm^2 for metallic SWNTs (short-dashed curve). Also plotted (open squares) are the data for the ~ 1580 cm^{-1} Lorentzian peak that is sometimes observed in metallic SWNTs.

BWF peak ω_G^- from the 16 isolated metallic SWNTs. Note that ω_G^+ does not show a diameter-dependent behavior, but always appears at about 1591 cm^{-1} for the SWNT diameter range observed, just as for semiconducting tubes. The BWF peak ω_G^- is more dispersive than the corresponding lower-frequency ω_G^- peak for isolated semiconducting SWNTs. Also ω_G^- for metallic SWNTs seems to extrapolate to 1591 cm^{-1} for $1/d_t \rightarrow 0$, just as for semiconducting SWNTs. The frequency of the ω_G^- feature for metallic SWNTs can also be very well fit with the simple equation $\omega_G^- = \omega_G^+ - C_M/d_t^2$, but with a different value for the constant, namely, $C_M = 79.5$ cm^{-1} nm^2. Furthermore, some metallic SWNTs exhibit another peak at about 1580 cm^{-1}, independent of d_t, and these data points are indicated in Fig. 3 by open squares.

B. Discussion

To our best knowledge, the first work about the *G*-band frequency dependence on SWNT diameter was published by Kasuya *et al.*,[10] and they reported an increase in the splitting of the *G*-band modes with decreasing nanotube diameter d_t. They compared their measurements on SWNT bundles having different diameter distributions with the splittings expected for the $E_1(E_{1g})$ and $E_2(E_{2g})$ modes due to zone folding of the graphite Brillouin zone into the nanotube Brillouin zone, and they showed good qualitative agreement between experiment and theory.[10] However, the zone folding scheme cannot alone explain the splitting observed for the $A(A_{1g})$ symmetry *G*-band modes in nanotubes, since these modes come from the center of the graphite Brillouin zone.[1,6]

In previous work,[9] we proposed that the curvature of the nanotubes leads to different force constants for *G*-band modes with atomic vibrations along the tube axis as compared to modes with vibrations in the circumferential direction. *G*-band mode calculations using the bond-polarization model, considering atomic interactions up to fourth-nearest neighbors, show that the orthogonal eigenvectors can be taken either along the tube axis or perpendicular to it, independent of SWNT chiral angle.[11,12]

The two peaks observed experimentally in the resonant *G*-band spectra from the *metallic* nanotubes that are present in SWNT bundles have also been interpreted in terms of circumferential and axial vibrations.[18] The higher-frequency ω_G^+ peak for metallic SWNTs has a Lorentzian line shape, but it is generally broader than the 1591 cm^{-1} peak in semiconducting tubes and it appears at the graphite frequency 1582 cm^{-1} in SWNT bundles. The lower-frequency ω_G^- peak for metallic SWNTs is much broader, and exhibits an asymmetric BWF line shape,[15,16,18] both at the single SWNT level and in SWNT bundles. The line shape (frequency, width, intensity, and asymmetry) of the BWF line in SWNT bundles depends on the strength of the coupling of the discrete phonon ω_G^- to an electronic continuum, and the line shape was shown to depend on nanotube diameter.[18] Therefore, the coupling between the lower-frequency phonon ω_G^- for displacements in the circumferential direction and the electronic continuum for metallic SWNTs increases with decreasing d_t, i.e., with increasing tube curvature.

Insight into the dispersive/nondispersive nature relative to the diameter dependence of the ω_G^-/ω_G^+ peaks in the *G* band of both metallic and semiconducting SWNTs can be obtained by considering the circumferential vs axial displacements of the *G*-band modes.[10–12] The force constants for the ω_G^- modes with atomic vibrations along the circumferential direction are strongly dependent on nanotube curvature, while the force constants for the ω_G^+ modes, where the atomic vibrations occur along the tube axis direction, do not depend on d_t. As stated above, the extra downshift of the BWF peak in metallic SWNTs compared to semiconducting SWNTs is attributed to the phonon-plasmon coupling in the metallic SWNTs.[18] Comparing the observed dispersion with d_t for the BWF ω_G^- peak for the isolated SWNTs reported here with the previously reported ω_{BWF} dispersion with d_t for SWNT bundles,[18] we see that the less accurate determination of the BWF frequency dispersion with d_t previously reported for SWNT bundles[18] was underestimated.

A surprising result is the observation that for large tube diameters, the BWF mode frequencies for isolated SWNTs extrapolate to 1591 cm^{-1}, and not to 1582 cm^{-1}, the graphite value.[1] A possible explanation for this result is the interaction between adjacent graphene layers in three dimensional (3D) graphite that might be responsible for a ~ 9 cm^{-1} downshift in the frequency of the Raman-active tangential mode from 1591 cm^{-1} for the 2D graphene sheet to 1582 cm^{-1} for 3D graphite. However, it is important to comment on the presence of two peaks in the upper *G* band for isolated metallic SWNTs, one at about 1591 cm^{-1} and another at around 1580 cm^{-1} (see Fig. 2). The frequency for the ~ 1580 cm^{-1} Lorentzian peak is also plotted in Fig. 3 with open squares. The ~ 1580 cm^{-1} peak is not always present in the Raman spectra for isolated SWNTs (see Fig.

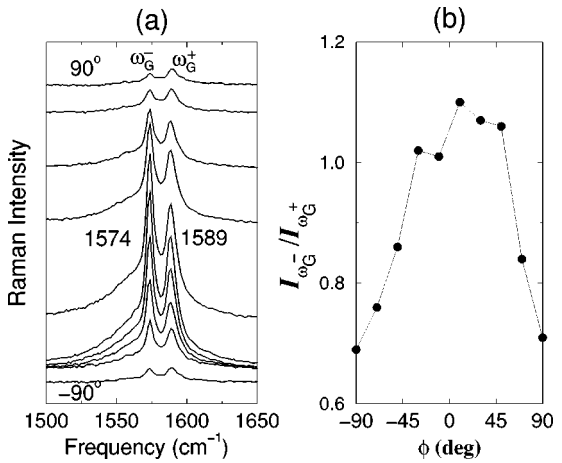

FIG. 4. (a) plots the *G*-band spectra for 10 different values of the angle ϕ between the light polarization direction and the nanotube axis. (b) plots the integrated intensity ratio $I_{\omega_G^-}/I_{\omega_G^+}$ as a function of ϕ.

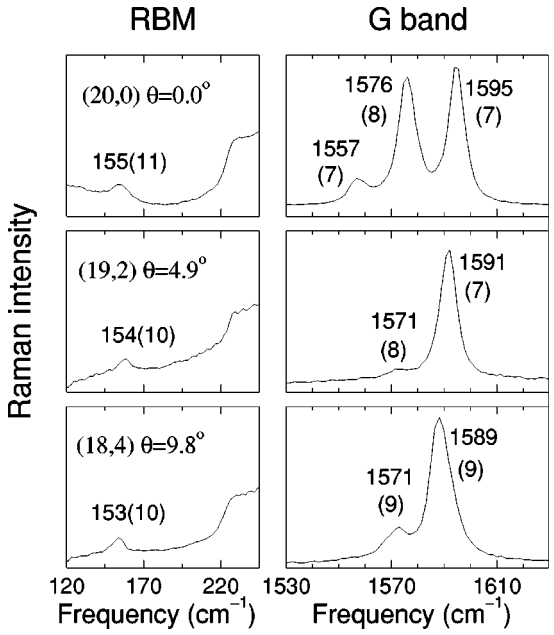

FIG. 5. The RBM and *G*-band Raman spectra for three isolated semiconducting SWNTs with similar diameters ($d_t \sim 1.60$ nm) that are resonant with the laser ($E_{\text{laser}} = 2.41$ eV) at three different spots on the sample. The frequencies (linewidths) of the intense peaks are displayed in cm^{-1}. The shoulder observed to the right side of the RBM spectral feature comes from the Si substrate. The tentative (n,m) indices and respective chiral angles θ are also displayed for each nanotube.

3), and it is generally of much smaller intensity than the ~ 1591 cm^{-1} peak. In the case of metallic SWNTs in a bundle, the strongest Lorentzian line in the *G*-band Raman spectra is generally much broader, with a peak appearing at 1582 cm^{-1}. More experimental work is necessary to clarify the presence of this ~ 1580 cm^{-1} peak that is found for some metallic SWNTs, but not for others.

IV. *G*-BAND INTENSITY DEPENDENCE ON POLARIZATION SCATTERING GEOMETRY, DIAMETER, AND CHIRALITY

A. Experimental results

Regarding the integrated intensities $I_{\omega_G^+}$ and $I_{\omega_G^-}$ for the two most intense *G*-band features, important and relevant experimental results come from polarization measurements on isolated SWNTs. Figure 4(a) plots the *G*-band spectra as a function of the angle ϕ between the polarization direction of the incident light and the nanotube axis. The scattered light was not analyzed. The general *G*-band intensity behavior is dictated by the antenna effect, whereby the optical absorption is strongly suppressed when the light is polarized perpendicular to the nanotube axis.[22–26] The same is valid for the RBM feature observed at 152 cm^{-1}. However, it is clear from Fig. 4(a) that the integrated intensity ratio $I_{\omega_G^-}/I_{\omega_G^+}$ changes significantly for light polarized at different angles ϕ to the nanotube axis. Figure 4(b) plots $I_{\omega_G^-}/I_{\omega_G^+}$ vs ϕ, showing that for light polarized along the tube axis, where the resonance effect is stronger, $I_{\omega_G^-}$ is larger than $I_{\omega_G^+}$, while for light polarized perpendicular to the nanotube axis, the ω_G^- peak is strongly suppressed, $I_{\omega_G^-}$ being smaller than $I_{\omega_G^+}$.

The relative intensity of the dominant ω_G^- and ω_G^+ features was also observed to vary from one spectrum to another (see Fig. 5, and Refs. 11 and 33). We show in Fig. 5 the RBM and the *G*-band spectra for three different isolated semiconducting SWNTs coming from three different light spots on the sample. These three tubes all exhibit similar diameters ($d_t \sim 1.60$ nm), and the (n,m) indices for each nanotube were tentatively determined on the basis of their RBM spectra[28] to yield the diameter and chiral angle for each tube. For all three nanotubes in Fig. 5, the incident laser is resonant with the E_{44}^S electronic transition. The spectra in Fig. 5 show that the relative intensities between the ω_G^- and the ω_G^+ modes are quite different from one spectrum to another.

However, it is important to mention that we did not choose three spectra with $d_t \sim 1.60$ nm by chance. Only a few SWNTs (corresponding to about 10% of the spectra that were taken) and specially those with d_t in the range $d_t = 1.60 \pm 0.05$ nm, exhibit *G*-band spectra with either unusually high or unusually low intensities for the ω_G^- peak in comparison to the intensity of the ω_G^+ peak. In general, for most of the semiconducting *G*-band spectra that we have studied in this work (and also for most of the spectra for which we have with no associated RBM features), the ratio $I_{\omega_G^-}/I_{\omega_G^+}$ is in the range 0.1 to 0.3, and the spectral profile looks like the *G*-band feature usually seen for SWNT bundles[1] when semiconducting tubes are resonantly contributing to the Raman spectra, such as for the (18,4) tube in Fig. 5. In Sec. IV B, we discuss why the special *G*-band spectra in Fig. 5 only occur under very special situations.

B. Discussion

From Fig. 4, it is clear that different relative intensities between the *G*-band modes are related to the polarization

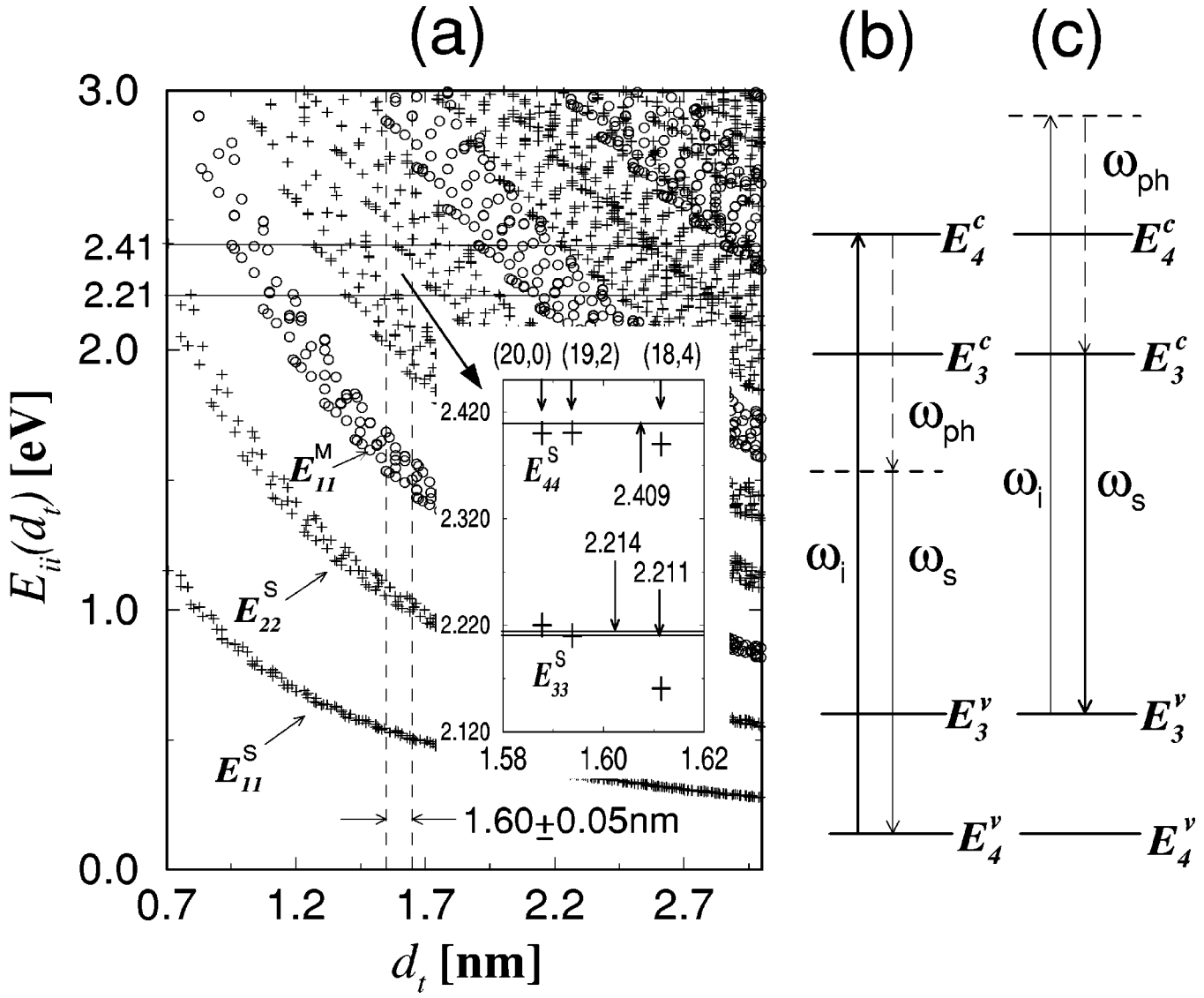

FIG. 6. (a) Plot of the electronic transitions E_{ii} for SWNTs with diameters between $0.7<d_t<3$ nm as a function of diameter, obtained from tight-binding calculations (Ref. 6) with $\gamma_0=2.90$ eV. Crosses give the E_{ii}^S values for semiconducting SWNTs and circles give E_{ii}^M values for metallic SWNTs. The inset shows an enlargement of the region where the crosses correspond to the E_{33}^S and E_{44}^S electronic transitions for the three SWNTs shown in Fig. 5. The vertical lines indicate the incident photon energy $E_{\text{laser}}=2.409$ eV, and the scattered photon energies for the ω_G^+ ($E_{\text{laser}}-E_{\text{ph}}=2.211$ eV) and ω_G^- ($E_{\text{laser}}-E_{\text{ph}}=2.214$ eV) scattering processes. (b) and (c) show schematic figures for the two possible scattering processes for SWNTs with $d_t=1.60\pm0.05$ nm [vertical dashed lines in (a)], where resonance can occur with either (b) the incident photon, or (c) the scattered photon ($E_{\text{laser}}-E_{\text{ph}}\sim2.41-0.20=2.21$ eV).

scattering geometry. However, in the last section we showed that the special *G*-band spectra observed in this work only occur under very special situations. For semiconducting SWNTs resonant with $E_{\text{laser}}=2.41$ eV, special *G*-band spectra are observed only for tubes with diameters in the range $d_t=1.60\pm0.05$ nm. We analyze here the case for semiconducting SWNTs recorded with $E_{\text{laser}}=2.41$ eV because we have by far the most complete data set for tubes resonant with this E_{laser} (35 of the 46 semiconducting SWNTs are resonant with $E_{\text{laser}}=2.41$ eV).

Bond-polarization theory for the Raman tensor predicts that the matrix elements for the different A, E_1, and E_2 *G*-band modes depend on chiral angle,[11,12] and this nonresonant theory provided a tentative explanation for the observation of different $I_{\omega_G^-}/I_{\omega_G^+}$ ratios for different SWNTs.[11,12,33] However, considering the top spectra in Fig. 5, the *G*-band peaks at 1557 cm^{-1} (E_2 symmetry) and 1576 cm^{-1} ($A+E_1$ symmetry) (Ref. 9) are both enhanced, in disagreement with predictions from the bond-polarization theory.[11,12] The fact that unusual $I_{\omega_G^-}/I_{\omega_G^+}$ intensity ratios were observed only for tubes with $d_t=1.60\pm0.05$ nm ($E_{\text{laser}}=2.41$ eV) cannot be explained by bond-polarization theory. Furthermore, the polarization dependence shown in Fig. 4 strongly suggests that the unusually strong $I_{\omega_G^-}$ intensity for this SWNT is related to the *resonant nature* of the Raman-scattering process, via the antenna effect.[23–26] As we discuss below, the present study on 62 isolated SWNTs

TABLE I. Mode frequencies (cm^{-1})/energy (eV) for the scattered photons for the different *G*-band features observed for the three SWNTs shown in Fig. 5. We use here $E_{laser}=2.409$ eV to calculate $E_{laser}-E_{ph}$. Also displayed are the observed RBM frequency ω_{RBM} (cm^{-1}), and the d_t (nm), θ (degrees), $248/d_t$ (cm^{-1}), and E_{ii}^S (eV) [$i=3,4$] values for each of the SWNTs. Here we see that E_{33}^S for (20,0) is closer to ω_G^- and ω_{E_2}, while E_{33}^S for (19,2) is closer to ω_G^+ (see boldface numbers).

(n,m)	(20,0)	(19,2)	(18,4)
d_t	1.59	1.59	1.61
θ	0.0	4.9	9.8
$248/d_t$	156.2	155.6	153.9
E_{33}^S/E_{44}^S	**2.22**/2.40	**2.21**/2.40	2.16/2.39
ω_{RBM}	155	154	153
$\omega_G^+/(E_{laser}-E_{ph})$	1595/2.211	1591/**2.211**	1589/2.212
$\omega_G^-/(E_{laser}-E_{ph})$	1576/**2.214**	1571/2.214	1571/2.214
$\omega_{E_2}/(E_{laser}-E_{ph})$	1557/**2.216**		

shows that the *G*-band spectra observed in Fig. 5 are strongly affected by the resonant nature of the Raman-scattering process in SWNTs and by the dependence of the resonance process on chiral angle.

Figure 6(a) shows the electronic transitions E_{ii} for SWNTs as a function of diameter. The $E_{laser}=2.41$ eV laser excitation energy is shown by a horizontal line, as well as the energy for the Stokes-scattered light $E_{laser}-E_{ph}\sim 2.41-0.20=2.21$ eV. Note that the special situation $d_t=1.60\pm 0.05$ nm [vertical dotted lines in Fig. 6(a)], for which the special *G*-band modes in Fig. 5 are observed, corresponds to a situation where E_{44}^S satisfies the resonance condition for the incident photon, while E_{33}^S satisfies the resonance condition with the scattered photon. Therefore, since in this work we consider only SWNTs in resonance with the incident light, we conclude that special *G*-band spectra are observed in this first-order process when the *scattered* photon is also in resonance with a SWNT interband transition.

Before continuing our analysis of the *G* bands, it is important to make it clear that the process discussed here is not a multiple resonance process. In a multiple resonance process, one photon is resonantly absorbed by the material, exciting a real electronic transition, and an internal scattering process(es) brings the electron to a different real state, and finally the electron decays back to the original state, resonantly emitting the scattered photon.[34] In the case discussed here, resonances with the incident photon and with the scattered photon are two independent processes represented in Figs. 6(b) and 6(c). In the process in Fig. 6(b), one photon is absorbed by one electron in the valence band E_4^v, and the electron is excited by an energy E_{44}^S to the conduction band E_4^c (resonant process); a *G*-band phonon brings the electron to a virtual state, and finally the electron decays to the original state E_4^v (nonresonant process), emitting the scattered photon. In the process in Fig. 6(c), one photon is absorbed by one electron in the valence band E_3^v, the electron is excited to a virtual state (nonresonant process), a *G*-band phonon brings the electron from the virtual state to an actual conduction-band state E_3^c, and the electron then lowers its energy by E_{33}^S to the original state E_3^v (resonant process), emitting the scattered photon. Both processes shown in Figs. 6(b) and 6(c) are single first-order resonant processes that are energetically possible for SWNTs with diameters in the range $d_t=1.60\pm 0.05$ nm that are excited with $E_{laser}=2.41$ eV. The two processes can occur independently in the same nanotube, and since E_{laser} and E_{ph} are each the same in the two processes, the scattered photon $E_{laser}-E_{ph}$ will have the same energy (same Stokes frequency), and the total intensity of the Raman signal will be given by the sum of the two resonant contributions.[35]

To understand the special *G*-band spectra shown in Fig. 5, it is important to consider that (i) the electronic transition energy E_{ii} is different for different SWNTs, depending on their chirality due to the trigonal warping effect;[36] (ii) the phonon energy E_{ph} is different for different ω_G frequency modes, such as ω_G^+ (1591 $cm^{-1}=198$ meV) and ω_G^- (1571 $cm^{-1}=195$ meV), and thus the energy $E_{laser}-E_{ph}$ for the scattered photon will also be different for different *G*-band modes. Therefore, for different SWNTs excited with the same E_{laser} and having almost the same d_t, different phonons may be enhanced differently by a resonance Raman process occurring with the scattered photons. The inset to Fig. 6(a) and Table I illustrate this picture, as we discuss below.

From their RBM features and their *D*-/*G*′-band spectra,[28,30,31] we tentatively assign the tubes shown in Fig. 5, from the top to the bottom as (20,0), (19,2), and (18,4), and this is summarized in Table I. Although the three SWNTs have similar diameters, they exhibit different chiral angles (see Fig. 5), and therefore, due to the trigonal warping effect, they exhibit different E_{ii} values [see Table I and the inset to Fig. 6(a)]. The frequencies for the various *G*-band peaks and the expected scattered photon energies are also displayed in Table I. In the case of the (20,0) and (19,2) SWNTs, the E_{33}^S values are within ~ 10 meV of the energies of the scattered photons ($E_{laser}-E_{ph}\sim 2.21$ eV), while for the (18,4) SWNT, the E_{33}^S value is far from the scattered photon energy (~ 50 meV). Although the tight-binding calculation[6] is not accurate to meV precision, we can say that in the case of the (20,0) SWNT, E_{33}^S is closer to the scattered photon energy involving ω_G^- ($E_{laser}-E_{ph}=2.409-0.195=2.214$ eV), while in the case of the (19,2) SWNT, E_{33}^S is closer to the scattered photon energy involving ω_G^+ ($E_{laser}-E_{ph}=2.409-0.198=2.211$ eV) [see inset to Fig. 6(a)]. Note that the lowest-frequency mode at 1557 cm^{-1} (E_2 symmetry) (Refs. 9 and 27) for the (20,0) SWNT is also enhanced by the scattered photon resonance that is close to E_{33}^S, and the E_2-symmetry *G*-band peak can be clearly observed [see the *G*-band spectrum for the (20,0) SWNT in Fig. 5]. The observations show higher relative enhancement for ω_G^- for the (20,0) SWNT, higher relative enhancement for ω_G^+ for the (19,2) SWNT, and the usual line shape for the (18,4) SWNT, consistent with predictions for the scattered photon resonance based on the tentative (n,m) assignments. Since the

energy difference between modes in the *G* band is only a few meV (24 cm^{-1} is equivalent to 3 meV) the observation of this resonance effect indicates that the resonance window is sharp (less than 10 meV), in agreement with previous works.[3,37]

The polarization results shown in Fig. 4 confirm the identification of the unusually high intensity for the ω_G^- mode as a special resonance effect. The intensity of the *G*-band modes depends on the resonance condition (how close the incident and scattered photons are to the electronic transitions E_{ii}), and depends on the antenna effect[22–26] shown in Fig. 4. From $\phi=90°$ to $\phi=0°$, $I_{\omega_G^-}$ in Fig. 4 increases by a factor of 17, while $I_{\omega_G^+}$ increases by a factor of 8. The fact that the antenna effect is two times stronger for the ω_G^- peak than for the ω_G^+ peak is in agreement with our explanation that two terms (incident and scattered photons) are contributing to the observed Raman intensity of the ω_G^- peak for this particular tube. Very few tubes are expected to exhibit this effect, in agreement with the observation of $0.1 < I_{\omega_G^-}/I_{\omega_G^+} < 0.3$ for ~90% of the observed spectra on isolated SWNTs.

By using an excitation laser energy of $E_{\text{laser}}=1.58$ eV, a similar effect (incident and scattered photons are independently resonant with different electronic transitions) should be observable only for tubes with d_t very close to 2.5 nm. However, it is very difficult to observe a clear RBM signal for tubes with such a large diameter. From the several spectra acquired with $E_{\text{laser}}=1.58$ eV, the few nanotubes that show special *G*-band spectra do not exhibit an associated RBM peak, which means that the resonance occurs with the scattered photon. Very few spectra of isolated SWNTs have been acquired so far with $E_{\text{laser}}=2.54$ eV. Among those that have been acquired, none shows special *G*-band spectra. From our model, special *G*-band spectra should be seen for SWNTs with $d_t \sim 1.48$ nm and $d_t \sim 2.50$ nm using laser energy of 2.54 eV.

Metallic SWNTs also show different relative intensities between the different components of the *G* band (see, for example, Fig. 5 in Ref. 33). Although the different E_{ii}^M subbands are distant in energy by much more than the *G*-band phonon energies [see Fig. 6(a)], metallic SWNTs exhibit a van Hove singularity splitting due to the trigonal warping effect,[36] and the dependence of the *G* band intensities on chiral angle can in such cases also be seen. However, the coupling between the ω_G^- mode with plasmons is another factor that must be considered for metallic SWNTs. The Lorentzian peak appearing at ~ 1580 cm^{-1} for some metallic SWNTs and not for others is another point that must be clarified and may be related to chirality. Further theoretical and experimental work is necessary to address the problem of the chirality dependence of the *G* band for metallic SWNTs.

V. CONCLUSION

We studied the *G*-band resonant Raman spectra of isolated single-wall carbon nanotubes (SWNTs) prepared by the CVD method on a Si/SiO_2 substrate. By using a very low-density sample and choosing SWNTs resonant with the incident laser, we succeeded in observing the RBM and the *G* band from the same SWNT. Making use of the tentative (n,m) assignments obtained by measuring the RBM spectra,[28] we identify the dependence of the *G*-band spectra on diameter and chirality, thus giving detailed information on the *G*-band Raman spectra at the single-nanotube level, separately, for semiconducting and metallic SWNTs. The tentative (n,m) assignment was performed on 16 different metallic and 46 semiconducting SWNTs resonant with several different electronic transitions E_{ii}, and these (n,m) values are used to label the spectra.

The *G* band exhibits two main features ω_G^+ and ω_G^-. The ω_G^+ peak always appears at around 1591 cm^{-1} for both semiconducting and metallic SWNTs, independent of diameter. The ω_G^- peak is diameter dispersive, and obeys the relation $\omega_G^- = \omega_G^+ - C/d_t^2$, with $C=C_S=47.7$ cm^{-1} nm^2 for semiconducting SWNTs and $C=C_M=79.5$ cm^{-1} nm^2 for metallic SWNTs. This diameter-dependent frequency behavior can be understood on the basis of the effect of tube curvature and of the tangential vs circumferential character of the vibrational modes. No dependence of the *G*-band frequencies ω_G^+ and ω_G^- on chiral angle was observed. Some metallic SWNTs exhibit an additional peak at around 1580 cm^{-1}, which needs further study.

The relative intensities of the *G*-band features were found to vary from one tube to another with $I_{\omega_G^-}/I_{\omega_G^+}$ lying in the range 0.1–0.3 for most of the observed SWNTs (about 90%). However, when the resonance occurs with the scattered photons, the energy difference between the electronic transition E_{ii} and the scattered photon energy $E_{\text{laser}}-E_{\text{ph}}$ will be different for different frequency phonons (ω_G^- and ω_G^+) associated with different (n,m) SWNTs. If the van Hove singularity of a specific (n,m) SWNT happens to be very close to $E_{\text{laser}}-E_{\text{ph}}$ for one of the *G*-band modes, it will be this particular phonon mode that will be strongly enhanced, giving rise to special *G*-band profiles.

ACKNOWLEDGMENTS

The authors A.J. and A.G.S.F. acknowledge financial support from the Brazilian agencies CNPq and CAPES. Part of the experimental work was performed at Boston University at the photonics center, operated in conjunction with their Department of Physics and Department of Electrical and Computer Engineering. This work also made use of the MRSEC shared facilities at Massachusetts Institute of Technology (MIT), supported by the National Science Foundation (NSF) under Grant No. DMR-9400334 and NSF laser facility Grant No. 97-08265-CHE. The MIT authors acknowledge support under NSF Grant Nos. DMR 01-16042, INT 98-15744, and INT 00-00408. R.S. acknowledges a Grant-in-Aid (No. 13440091) from the Ministry of Education, Japan.

*Present address: Department of Physics, Rice University, Houston, TX.
[1] M. S. Dresselhaus and P. C. Eklund, Adv. Phys. **49**, 705 (2000).
[2] S. Bandow, S. Asaka, Y. Saito, A. M. Rao, L. Grigorian, E. Richter, and P. C. Eklund, Phys. Rev. Lett. **80**, 3779 (1998).
[3] M. Milnera, J. Kürti, M. Hulman, and H. Kuzmany, Phys. Rev. Lett. **84**, 1324 (2000).
[4] A. M. Rao, P. C. Eklund, S. Bandow, A. Thess, and R. E. Smalley, Nature (London) **388**, 257 (1997).
[5] M. A. Pimenta, A. Marucci, S. D. M. Brown, M. J. Matthews, A. M. Rao, P. C. Eklund, R. E. Smalley, G. Dresselhaus, and M. S. Dresselhaus, J. Mater. Res. **13**, 2396 (1998).
[6] R. Saito, G. Dresselhaus, and M. S. Dresselhaus, *Physical Properties of Carbon Nanotubes* (Imperial College Press, London, 1998).
[7] D. Kahn and J. P. Lu, Phys. Rev. B **60**, 6535 (1999).
[8] R. Saito, T. Takeya, T. Kimura, G. Dresselhaus, and M. S. Dresselhaus, Phys. Rev. B **57**, 4145 (1998).
[9] A. Jorio, G. Dresselhaus, M. S. Dresselhaus, M. Souza, M. S. S. Dantas, M. A. Pimenta, A. M. Rao, R. Saito, C. Liu, and H. M. Cheng, Phys. Rev. Lett. **85**, 2617 (2000).
[10] A. Kasuya, Y. Sasaki, Y. Saito, K. Tohji, and Y. Nishina, Phys. Rev. Lett. **78**, 4434 (1997).
[11] R. Saito, A. Jorio, J. H. Hafner, C. M. Lieber, M. Hunter, T. McClure, G. Dresselhaus, and M. S. Dresselhaus, Phys. Rev. B **64**, 085312 (2001).
[12] R. Saito, A. Jorio, G. Dresselhaus, and M. S. Dresselhaus, in *The 25th International Conference on The Physics of Semiconductors, Osaka, 2000*, edited by N. Miura and T. Ando (Springer, Berlin, 2000) p. 1629.
[13] M. Damnjanović, I. Milosević, T. Vuković, and R. Sredanović, Phys. Rev. B **60**, 2728 (1999).
[14] O. E. Alon, Phys. Rev. B **63**, 201403(R) (2001).
[15] H. Kataura, Y. Kumazawa, Y. Maniwa, I. Umezu, S. Suzuki, Y. Ohtsuka, and Y. Achiba, Synth. Met. **103**, 2555 (1999).
[16] L. Alvarez, A. Righi, T. Guillard, S. Rols, E. Anglaret, D. Laplaze, and J.-L. Sauvajol, Chem. Phys. Lett. **316**, 186 (2000).
[17] Z. Yu and L. E. Brus, J. Phys. Chem. **104**, 1995 (2000).
[18] S. D. M. Brown, A. Jorio, P. Corio, M. S. Dresselhaus, G. Dresselhaus, R. Saito, and K. Kneipp, Phys. Rev. B **63**, 155414 (2001).
[19] M. A. Pimenta, A. Marucci, S. A. Empedocles, M. G. Bawendi, E. B. Hanlon, A. M. Rao, P. C. Eklund, R. E. Smalley, G. Dresselhaus, and M. S. Dresselhaus, Phys. Rev. B **58**, R16 016 (1998).
[20] P. M. Rafailov, H. Jantoljak, and C. Thomsen, Phys. Rev. B **61**, 16 179 (2000).
[21] S. D. M. Brown, P. Corio, A. Marucci, M. S. Dresselhaus, M. A. Pimenta, and K. Kneipp, Phys. Rev. B **61**, R5137 (2000).
[22] H. Ajiki and T. Ando, Physica B **201**, 349 (1994).
[23] G. S. Duesberg, I. Loa, M. Burghard, K. Syassen, and S. Roth, Phys. Rev. Lett. **85**, 5436 (2000).
[24] J. Hwang, H. H. Gommans, A. Ugawa, H. Tashiro, R. Haggenmueller, K. I. Winey, J. E. Fischer, D. B. Tanner, and A. G. Rinzler, Phys. Rev. B **62**, R13 310 (2000).
[25] Z. Yu and L. E. Brus, J. Phys. Chem. B **105**, 1123 (2001).
[26] A. Jorio, A. G. Souza Filho, V. W. Brar, A. K. Swann, M. S. Ünlü, B. B. Goldberg, A. Righi, J. H. Hafner, C. M. Lieber, R. Saito, G. Dresselhaus, and M. S. Dresselhaus, Phys. Rev. B **65**, 121402 (2002).
[27] C. Fantini, M. A. Pimenta, M. S. S. Dantas, D. Ugarte, A. M. Rao, A. Jorio, G. Dresselhaus, and M. S. Dresselhaus, Phys. Rev. B **63**, 161405 (2001).
[28] A. Jorio, R. Saito, J. H. Hafner, C. M. Lieber, M. Hunter, T. McClure, G. Dresselhaus, and M. S. Dresselhaus, Phys. Rev. Lett. **86**, 1118 (2001).
[29] The proportionality constant 248 cm^{-1} nm differs by less than 5% from theoretical predictions [J. Kürti *et al.*, Phys. Rev. B **58**, R8869 (1998); D. Sanchez-Portal *et al.*, *ibid.* **59**, 12 678 (1999)].
[30] A. G. Souza Filho, A. Jorio, G. Dresselhaus, M. S. Dresselhaus, R. Saito, A. K. Swan, M. S. Ünlü, B. B. Goldberg, J. H. Hafner, C. M. Lieber, and M. A. Pimenta, Phys. Rev. B **65**, 035404 (2002).
[31] A. G. Souza Filho, A. Jorio, G. Dresselhaus, M. S. Dresselhaus, Anna K. Swan, M. S. Ünlü, B. B. Goldberg, R. Saito, J. H. Hafner, C. M. Lieber, and M. A. Pimenta, Phys. Rev. B **65**, 085417 (2002).
[32] J. H. Hafner, C. L. Cheung, T. H. Oosterkamp, and C. M. Lieber, J. Phys. Chem. B **105**, 743 (2001).
[33] Z. Yu and L. E. Brus, J. Phys. Chem. B **105**, 743 (2001).
[34] R. M. Martin and L. M. Falicov, Top. Appl. Phys. **8**, 79 (1983).
[35] Figures 6(b) and 6(c) are schematic diagrams useful for understanding the physics responsible for the different intensities of the *G*-band components discussed here. However, for a quantitative description of the processes (e.g., calculation of the transition probabilities), summation over all the possible processes which connect the initial and final states should be considered.
[36] R. Saito, G. Dresselhaus, and M. S. Dresselhaus, Phys. Rev. B **61**, 2981 (2000).
[37] A. Jorio, A. G. Souza Filho, G. Dresselhaus, M. S. Dresselhaus, R. Saito, J. H. Hafner, C. M. Lieber, F. M. Matinaga, M. S. S. Dantas, and M. A. Pimenta, Phys. Rev. B **63**, 245416 (2001).